

# The fermion sign problem in Gauss law sectors of quantum link models with dynamical matter

Pallabi Dey<sup>1, 2, \*</sup> Debasish Banerjee<sup>1, 3, †</sup> and Emilie Huffman<sup>4, ‡</sup>

<sup>1</sup>*Theory Division, Saha Institute of Nuclear Physics, 1/AF Bidhan Nagar, Kolkata 700064, India*

<sup>2</sup>*Homi Bhabha National Institute, Training School Complex, Anushaktinagar, Mumbai 400094, India*

<sup>3</sup>*School of Physics and Astronomy, University of Southampton, University Road, SO17 1BJ, UK*

<sup>4</sup>*Department of Physics and Center for Functional Materials,  
Wake Forest University, Winston-Salem, North Carolina 27109, USA*

(Dated: December 18, 2025)

The fermion sign problem poses a formidable challenge to the use of Monte Carlo methods for lattice gauge theories with dynamical fermionic matter fields. A meron cluster algorithm recently formulated for gauge fields represented as spin- $\frac{1}{2}$  quantum links coupled to a single flavour of staggered fermions samples only two of the exponentially many Gauss law (GL) sectors at low temperatures, making it possible to simulate either of those two GL sectors at zero temperature in polynomial time. In this article, we analytically identify GL sectors which can be simulated without encountering the fermion sign problem in arbitrary spatial dimensions. Using large-scale exact diagonalization and cluster Monte Carlo methods, we further explore the nature of phases in the GL sectors dominating at zero temperature. The vacuum states lie in sectors which satisfy a staggered Gauss law, in contrast to the zero GL sector familiar in particle physics. Moreover, we prove that while the ground state GL sectors do not suffer from the fermion sign problem, the usual zero-charge GL sector (often considered the physical sector) does. We outline the role of the magnetic energy in causing transitions between GL sectors. We expect our results to be valid for truncated Kogut-Susskind gauge theories, beyond quantum link models.

*Introduction.*— The fermion sign problem is one of the outstanding challenges in the ab-initio simulation of quantum field theories (QFT) with fermionic matter using Markov Chain Monte Carlo (MCMC) methods [1]. Monte Carlo methods rely on the interpretation of the exponentiated Euclidean action as Boltzmann weights for importance sampling. With fermions involved, the Boltzmann weights in the occupation number basis of the fermions (or the field basis) are not explicitly positive definite for individual configurations, giving rise to the sign problem. Consequently, physics at finite baryon chemical potential [2] or the Hubbard model at finite doping [3] suffer from a severe fermion sign problem.

There are multiple approaches to tackle sign problems [4–14], but the meron concept [15, 16] attacks the problem in a very direct way. The key idea is to first perform an analytic summation of certain fermionic world-line configurations to cancel those with equal and opposite signs, and subsequently to completely avoid generating such configurations during the importance sampling [17]. While the original meron proposal dealt with a single component of staggered fermions, generalizations involving multiple fermion species followed later [18]. Another very important direction involves incorporating gauge fields coupled to fermions [19, 20]. The microscopic Hamiltonian involving gauge fields has more constraints, due to superselection sectors specified by Gauss Laws, which make the application of the meron idea more challenging.

Adding gauge fields to fermions is a natural next step in the investigation of phase diagrams of models towards quantum chromodynamics. Another motivation for the

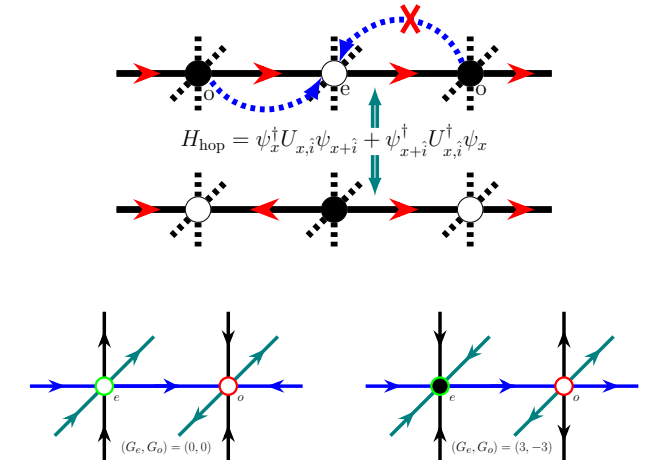


Figure 1. (Top): The fermion hop from left to right is accompanied by a  $\sigma^- (U^\dagger)$  operator on the link, causing the spin-1/2 electric flux to flip its orientation, while the right to left hop is accompanied by a  $\sigma^+ (U)$  operator on the link and is thus constrained by the state of the flux on the link. (Bottom): Examples of electric flux configurations belonging to two different Gauss Law sectors. The direction of the arrows on the links indicates the flux to be  $E_{x,i} = \pm \frac{1}{2}$ , while the filled (empty) sites indicate the site to be occupied (empty).

study of these models is provided by the rapidly evolving field of analog and digital quantum simulator experiments which can simulate constrained lattice gauge theories and spin models in  $d = 1, 2$  [21–34]. Some such constrained models that have been realized in analog quantum simulators are closely connected with quantum link

models (QLMs) [35], even the PXP model is the spin-1/2 quantum link Schwinger model. QLMs are generalized lattice gauge theories which realize exact gauge invariance using a finite-dimensional local Hilbert space for the gauge links [36, 37], and thus can be efficiently encoded in quantum simulators and computers [38]. Moreover, by choosing an appropriate representation of the gauge fields, or the fermion content, many QLMs can be mapped to pedagogical models in condensed matter physics, such as the quantum dimer model and the quantum spin ice [39–42].

Non-perturbative study of these models on large lattices theoretically requires advanced numerical techniques. While tensor network methods are extremely mature in  $d = 1$ , their viability in  $d > 1$  spatial dimensions are still limited. Therefore, it is urgently required to expand the repertoire of classical Monte Carlo algorithms which can address the static properties of these theories. Such investigations are very crucial not only for investigating ground state physics, serving as benchmarks for quantum computer implementations, but they also influence planning possible investigations for real-time dynamics on quantum computers. Further, many of these models show novel phenomena beyond traditional lattice gauge theories [41, 43], and could have intriguing technological implications.

Here we further explore  $U(1)$ -symmetric models of gauge fields and matter with meron cluster techniques and exact diagonalization (ED), specifically for  $d = 2$  and,  $d = 3$  spatial dimensions. The paper is organized as follows: after explaining the structure of the Hamiltonian and the Gauss Law, we examine the fermion world lines in different GL sectors, and analytically identify GL sectors where the fermionic sign problem is absent. Using large-scale ED, the low-energy physics and the nature of the ground states in different GL sectors that dominate at low temperatures is studied. We also study transitions between the GL sectors as the couplings are varied. We conclude with a discussion on how our results are applicable to truncated lattice gauge theories beyond QLMs.

*QLM Hamiltonian and Gauss Law sectors.*— The original meron concept was applied to a single-component fermionic species with nearest neighbour hopping, and interactions via a four-fermion coupling. When the gauge fields are coupled to fermions, a fermion hop across a link to a neighbouring site changes the flux on the link. If the theory uses a finite-dimensional flux representation, as in the QLM formulation, the hopping is constrained by the flux on the link (see fig. 1 (top)). In the occupation number basis for the fermions and the

electric flux basis for gauge fields, the Hamiltonian is:

$$H = -t \sum_{x,i} \left[ \left( \psi_x^\dagger U_{x,i} \psi_{x+i} + \text{h.c.} \right) - E_{x,i} (n_{x+i} - n_x) \right] + (V - t) \sum_{x,i} \left( n_x - \frac{1}{2} \right) \left( n_{x+i} - \frac{1}{2} \right) - \frac{t \cdot d \cdot \mathcal{V}}{4}. \quad (1)$$

The first term causes the fermion hopping simultaneously with the gauge field  $U_{x,i}$  ( $U_{x,i}^\dagger$ ) creating (annihilating) a unit of electric flux,  $E_{x,i}$ , on the link joining sites  $x$  and  $x+i$  as shown in fig. 1. Next is the so-called *designer* term equal in strength to the hopping and necessary for the meron concept to be applicable [19]. The third term is a density-density interaction at neighbouring sites, equivalent to a four-fermi coupling. We imagine the system in  $d$ -dimensions with spatial volume  $\mathcal{V}$ .

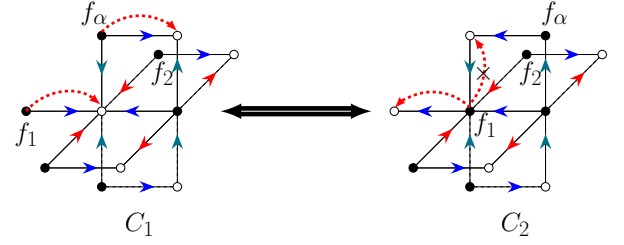


Figure 2. The orientation of the gauge links in the sector  $(3, -3)$  in  $d = 3$  do not allow the movement of fermions beyond one lattice spacing. Thus, positions of  $f_1$  and  $f_2$  cannot be switched by the action of the Hamiltonian.

Here we use the spin- $\frac{1}{2}$  representation for gauge fields, with two states for each link. Although any spin- $S$  representation is possible to maintain the  $U(1)$  gauge symmetry, the only known meron-cluster algorithm, for  $d > 1$ , is for spin- $\frac{1}{2}$ . This is also a maximally constrained system, likely to display exotic physics. There is evidence in  $d = 1$  that the continuum limit can be obtained with relatively low spin representations [44]. The local  $U(1)$  symmetry transformation is generated by the following Gauss Law operator:

$$G_x = n_x + \left( \frac{(-1)^x - 1}{2} \right) - \sum_i (E_{x,i} - E_{x-i,i}), \quad (2)$$

where  $(-1)^x$  is the site parity. It is easy to check that  $[G_x, H] = 0$ , which splits the physical Hilbert space into superselection sectors, labelled by eigenvalues of  $G_x$ . The staggered fermion occupation in eq. (2) is necessary for preserving the global charge conjugation symmetry and a charge neutral vacuum. Consequently, we use  $(G_e, G_o)$  to denote even and odd-site GL sectors locally. In fig. 1 (bottom), we show examples of flux configurations in two different GL sectors,  $(0, 0)$  and  $(3, -3)$ , which play a role in our investigation in  $d = 3$ .

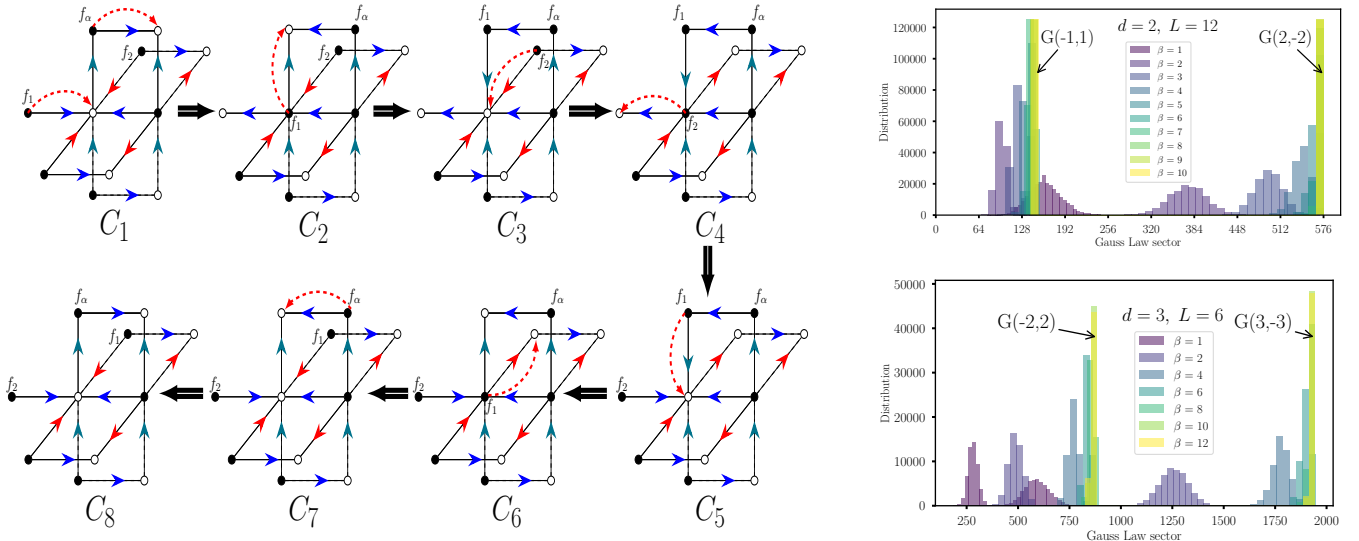


Figure 3. (Left): The GL constraints in the sector  $(2, -2)$  in  $d = 3$  are relaxed enough to allow fermions  $f_1$  and  $f_2$  to exchange positions with each other following the general prescription described in the text. (Right) The different GL sectors that are sampled by the QMC algorithm at different  $\beta$ . For low temperature (large  $\beta$ ) only the GL  $(d, -d)$  and its shifted partner arises.

Postponing a general discussion of global symmetries to the SM, we instead concentrate on the consequence of the discrete chiral symmetry, where all fermion and gauge operators are translated by one lattice spacing in a given direction. The two-site GL  $(G_e, G_o) = (n - \nabla \cdot E, n - 1 - \nabla \cdot E)$ , transforms as  $G_e \rightarrow G_o + 1, G_o \rightarrow G_e - 1$ . The Hilbert space for  $d = 2$  (square lattice) in the GL sector  $(0, 0)$  is constructed by solving  $n - \nabla \cdot E = 0$  and  $n - \nabla \cdot E = 1$  for even and odd sites respectively. The first equation has 6 (4) solutions with  $n = 0$  ( $n = 1$ ), while the second gives 4 (6) solutions with  $n = 0$  ( $n = 1$ ), and thus we have 10 (10) solutions for the GL sector  $(0, 0)$  on even (odd) sites when counting independently. For the shifted GL sector  $(1, -1)$ , the equations for the even and odd sites are interchanged, but the number of solutions are the same. This, together with the fact that the Hamiltonian does not connect the  $(0, 0)$  and the  $(1, -1)$  sector, establishes an isospectral relation between the two sectors. Similarly, the pairs  $[(2, -2)$  and  $(-1, 1)]$  and  $[(3, -3)$  and  $(-2, 2)]$  are isospectral, independent of spatial dimensions. More details are provided in the SM.

*Sign Problem in different sectors.*— We have studied the model in  $d = 2, 3$  with both ED and the meron algorithm [19]. While the constraining nature of gauge links prevent any permutation of fermionic worldlines in  $d = 1$  and therefore there is no sign problem in any GL sector, we do not have this restriction in  $d > 1$ , so we explore the fermion sign problem in  $d = 2, 3$  in different GL sectors. We outline our analytic arguments and the surprising results in this section, while independent numerical checks are provided in the SM.

Our key result can be stated simply: *the Gauss Law sector  $(d, -d)$  and its shift partner  $(-d + 1, d - 1)$  do*

*not suffer from the fermion sign problem, while all other sectors do.* Stated differently, the partition functions are identical if the fermions are replaced by (hardcore) bosons. The analytic proof proceeds by identifying two fermions in a spatial configuration and interchanging their positions by acting with the Hamiltonian, keeping the positions of all other fermions fixed.

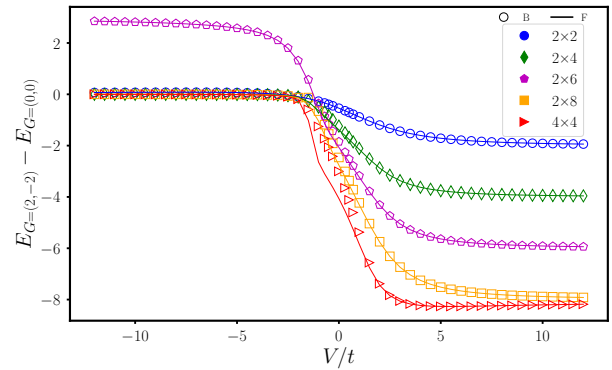


Figure 4. Ground state energy difference between the GL sectors  $(2, -2)$  and  $(0, 0)$  for bosons (open symbols) and fermions (solid lines) respectively in  $d = 2$ . While the fermionic and bosonic results are the same for the sector  $(2, -2)$ , there is a difference in the  $(0, 0)$  sector for  $V/t \sim 0$ , leading to the deviation between the two sets of data in that region.

Consider the sector  $(3, -3)$ , which has  $(7, 7)$  allowed solutions to the GL constraints, one of which is shown in fig. 2. We identify  $(f_1, f_2)$  as two fermions with positions  $(r_1, r_2)$ , and we also identify an auxiliary fermion  $f_\alpha$  at position  $r_\alpha$  which we will use to facilitate the interchange in positions of  $(f_1, f_2)$ . The procedure is to

move  $f_1$  to  $r_\alpha$  (by shifting  $f_\alpha$ ), while  $f_2$  is moved to  $r_1$ . It is then completed by pushing  $f_1$  to  $r_2$ , and  $f_\alpha$  is restored to its original location. As shown in fig. 2, just after a single hop of  $f_1$ , we encounter links (fixed by GL) which forbid further hopping of  $f_1$  — only the reverse hop back to  $r_1$  is allowed. Although the process is shown for one example, we have verified this to be the case for *all* configurations locally in the GL sector  $(3, -3)$  (and by extension to its shift partner). This is in contrast to the case of the sector  $(2, -2)$  shown in fig. 3 (left), where the above procedure works out. Thus, configurations  $C_1$  and  $C_8$  differ by an overall sign when computations are performed in this basis. It results in a severe sign problem in a QMC sampling, which can be potentially solved with the meron concept.

In the SM, this argument is outlined for the  $(0, 0)$  sector, particularly relevant in particle physics, where it suffers from a sign problem as well. Moreover, the discussion is also true in  $d = 2$ : the sector  $(2, -2)$  has no sign problem, but the  $(0, 0)$  has one. This analytic argument also explains why no sign problem was found in  $d = 1$  in [19]. Fig 3 (right) shows distributions of the different GL sectors obtained in the QMC algorithm at different temperatures for both  $d = 2, 3$ . Details of the QMC algorithm used are provided in the SM.

*Low energy physics.*— The next relevant question is the role of each GL sector at  $T \approx 0$ . With increase in temperature, matter-anti-matter pairs can be created as annealed disorder, and thus thermal fluctuations can connect different GL sectors. At zero temperature, the Hamiltonian in eq. (1), has the sector  $(d, -d)$  (and the shift partner) as the ground state for  $V/t > 0$  (as we show next). This phase (for any  $d$ ) consists of frozen fermions, which can locally hop, but can never get away.

In  $d = 2$ , using large-scale ED, we study the ground state at different  $V/t$  regimes for both (hardcore) bosonic and fermionic matter up to 48 DOF (16 matter sites and 32 gauge links). Using a Krylov-space based ED, system sizes till 72 DOF (i.e., lattices  $12 \times 2, 6 \times 4$ ) could be reached. Motivated to identify which GL sector forms the global ground state, fig. 4 plots the difference in ground state energies of the two GL sectors indicated in the subscript,  $E_{(2, -2)}^0 - E_{(0, 0)}^0$ , for bosonic and fermionic matter (the other sectors are higher in energy). The difference arises only in the regime  $V/t \sim 0$ , when particles can maximally hop making their exchange statistics manifest. Large (whether positive or negative)  $V/t$  values fix  $n_x$  values, making the bosonic or fermionic nature irrelevant. Except for a finite size effect on the  $2 \times 6$  ladder,  $E_{(2, -2)}^0$  is lower in energy for almost the entire regime, except for negative  $V/t$  when it is degenerate.

The chiral condensate ( $\langle \psi^\dagger \psi \rangle$ ) and the sum of staggered electric flux,  $\epsilon_{x,y}$ , defined in eq. (18), and plotted in fig. 5 help to explain the nature of the ground state. Pure fermions at  $V/t \gg 0$  would give rise to the charge-density

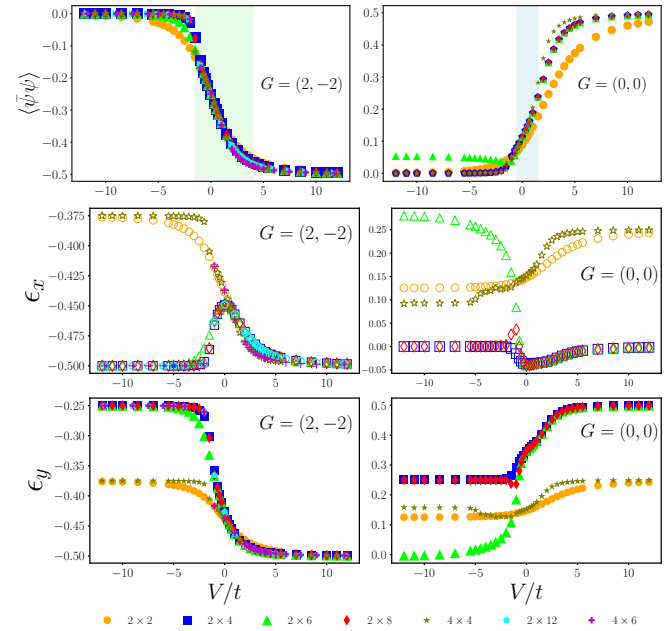


Figure 5. Top two figures show  $\langle \bar{\psi} \psi \rangle$  vs  $V/t$  in the two GL sectors in  $d = 2$ . The  $\mathbb{Z}_2$  chiral symmetry breaks for  $V/t \gg 0$  in both sectors, while phase separation occurs for  $V/t \ll 0$ . The shaded band for  $V/t \sim 0$  indicates a region where a liquid phase is suspected. The bottom two panels show  $\epsilon_{x,y}$  for each GL sector in  $d = 2$ . In  $(2, -2)$  the symmetric ordering of the flux causes both  $\epsilon_{x,y}$  to reach the same value for  $V/t > 0$  while due to phase separation at  $V/t < 0$ ,  $\epsilon_x$  and  $\epsilon_y$  have different values, also depending on whether it is a ladder or a square geometry. In GL sector  $(0, 0)$ , the ordering of the flux requires a larger unit cell, and is thus sensitive to a multiple of 2 vs 4.

wave (CDW) phase (spontaneous breaking of the discrete  $\mathbb{Z}_2$  chiral symmetry). Gauge fields explicitly break the  $\mathbb{Z}_2$  symmetry and the two CDW vacua belong to two different GL sectors, with equal and opposite (non-zero) values of the chiral condensate. For  $V/t \ll 0$ , both sectors have phase separated ground states featuring neighbouring sites that are empty on one side of the lattice, and filled on the other, causing the condensate to vanish. There is a narrow intermediate regime characterized by matter hopping, and finite size scaling (see SM) indicates that it may be a liquid phase. For the GL sector  $(0, 0)$  similar results have been obtained in [45–47].

The electric fluxes (see fig. 5 (bottom)) corroborate this understanding. The  $\mathbb{Z}_2$  symmetry breaking for  $V/t \gg 0$  causes both the staggered fluxes in  $x$  and  $y$  asymptote to the same value (in the  $(0, 0)$  sector the flux ordering is sensitive to  $L_y$  being a multiple of 2 or 4). For  $V/t \ll 0$ , the phase separation makes  $\langle \epsilon_x \rangle$  and  $\langle \epsilon_y \rangle$  depend on whether the system is square or rectangular, indicating a spontaneous breaking of discrete rotation symmetry. We provide a detailed understanding of the different phases in the SM.

We have also examined the role of including the mag-

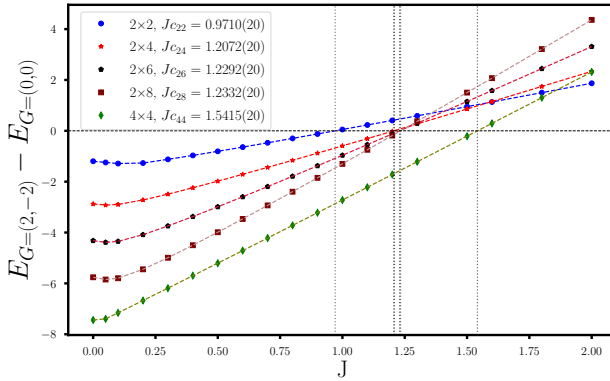


Figure 6. Transition between the  $(2, -2)$  and  $(0, 0)$  GL sectors as the magnetic coupling is increased.

netic energy term,  $-J \sum_{\square} (U_{\square} + U_{\square}^{\dagger})$ , to the Hamiltonian in eq. (1), for fermionic matter at  $V = 2t$ . Fig 6 (analogous to fig. 4 for both ladder and square systems) shows that although the GL sector  $(2, -2)$  is the ground state across *all* GL sectors, it undergoes a phase transition to the  $(0, 0)$  sector, beyond a critical coupling  $J_c$  when the magnetic field dominates. For ladder systems, we estimate  $J_c \approx 1.23(1)$  shown as dashed vertical line in fig. 6. For square systems,  $J_c$  is larger, but we expect it to be still  $O(1)$  based on the scaling for  $2 \times 2$  and  $4 \times 4$  systems. The  $6 \times 6$  lattice has a total of 108 DOF, and beyond the scope of our ED. The meron algorithm does not yet work for  $J \neq 0$ .

*Conclusions and Outlook.*— In this article, we have analyzed the fermion sign problem in different GL sectors of Abelian gauge theories with a finite dimensional Hilbert space. Although the explicit examples considered were spin- $\frac{1}{2}$  quantum links, the methods developed in the paper can be straightforwardly applied to a spin- $S$  link model or a truncated Kogut-Susskind Hamiltonian. While we have been successful in the construction of a cluster algorithm that works in the ground state GL without using the meron idea, it is a very interesting question to ask if the meron idea can be successfully utilized in order to cancel the sign problem in specific GL sectors such as  $(0, 0)$ . This is currently a work in progress by the authors.

The successful application of the meron in the other GL sectors will allow us to simulate the microscopic model of quantum electrodynamics (QED) in  $d = 2, 3$ . In  $d = 2$ , there are several results in the literature on QED3 [48–53] and our QMC algorithm can independently verify the existing results for the underlying QFT. Furthermore, the results presented here could also be used to benchmark quantum simulator experiments, particularly using Rydberg atoms [28, 54–56], and perhaps design quench experiments to understand dynamical properties of this model. In  $d = 3$ , search for the Coulomb phase of QED

found in Nature is a natural next step for investigation.

*Acknowledgements.*— We would like to thank Joao Pinto Barros, Thea Budde, Shailesh Chandrasekharan, Arnab Sen, and Uwe-Jens Wiese for useful discussions. D.B. would like to thank STFC (UK) consolidated grant ST/X000583/1 and continued support from the Alexander von Humboldt Foundation (Germany) in the context of the research fellowship for experienced researchers. We thank computing resources of SINP and DiRAC (computational facility for STFC) essential to derive these results.

\* pallabi.dey@saha.ac.in

† D.Banerjee@soton.ac.uk

‡ ehuffman@wfu.edu

- [1] Matthias Troyer and Uwe-Jens Wiese, “Computational complexity and fundamental limitations to fermionic quantum monte carlo simulations,” *Physical Review Letters* **94** (2005), 10.1103/physrevlett.94.170201.
- [2] Keitaro Nagata, “Finite-density lattice qcd and sign problem: Current status and open problems,” *Progress in Particle and Nuclear Physics* **127**, 103991 (2022).
- [3] Daniel P. Arovas, Erez Berg, Steven A. Kivelson, and Srinivas Raghu, “The hubbard model,” *Annual Review of Condensed Matter Physics* **13**, 239–274 (2022).
- [4] Congjun Wu and Shou-Cheng Zhang, “Sufficient condition for absence of the sign problem in the fermionic quantum monte carlo algorithm,” *Phys. Rev. B* **71**, 155115 (2005).
- [5] F. F. Assaad and T. C. Lang, “Diagrammatic determinantal quantum monte carlo methods: Projective schemes and applications to the hubbard-holstein model,” *Phys. Rev. B* **76**, 035116 (2007).
- [6] Shailesh Chandrasekharan, “Fermion bag approach to lattice field theories,” *Phys. Rev. D* **82**, 025007 (2010).
- [7] Marco Cristoforetti, Francesco Di Renzo, and Luigi Scorzato (AuroraScience Collaboration), “New approach to the sign problem in quantum field theories: High density qcd on a lefschetz thimble,” *Phys. Rev. D* **86**, 074506 (2012).
- [8] Emilie Fulton Huffman and Shailesh Chandrasekharan, “Solution to sign problems in half-filled spin-polarized electronic systems,” *Physical Review B* **89** (2014), 10.1103/physrevb.89.111101.
- [9] Emilie Huffman and Shailesh Chandrasekharan, “Solution to sign problems in models of interacting fermions and quantum spins,” *Phys. Rev. E* **94**, 043311 (2016).
- [10] Emilie Huffman and Shailesh Chandrasekharan, “Fermion bag approach to hamiltonian lattice field theories in continuous time,” *Phys. Rev. D* **96**, 114502 (2017).
- [11] Christof Gattringer and Kurt Langfeld, “Approaches to the sign problem in lattice field theory,” *Int. J. Mod. Phys. A* **31**, 1643007 (2016), arXiv:1603.09517 [hep-lat].
- [12] Lei Wang, Ye-Hua Liu, and Matthias Troyer, “Stochastic series expansion simulation of the  $t-v$  model,” *Phys. Rev. B* **93**, 155117 (2016).
- [13] Zi-Xiang Li and Hong Yao, “Sign-problem-free fermionic quantum monte carlo: Developments and applica-

tions,” *Annual Review of Condensed Matter Physics* **10**, 337–356 (2019), <https://doi.org/10.1146/annurev-conmatphys-033117-054307>.

[14] Christoph Gängten, Evan Berkowitz, Thomas Luu, Johann Ostmeyer, and Marcel Rodekamp, “Fermionic sign problem minimization by constant path integral contour shifts,” *Phys. Rev. B* **109**, 195158 (2024), [arXiv:2307.06785](https://arxiv.org/abs/2307.06785) [cond-mat.str-el].

[15] Shailesh Chandrasekharan and Uwe-Jens Wiese, “Meron cluster solution of a fermion sign problem,” *Phys. Rev. Lett.* **83**, 3116–3119 (1999), [arXiv:cond-mat/9902128](https://arxiv.org/abs/cond-mat/9902128).

[16] Hanqing Liu, Shailesh Chandrasekharan, and Ribhu K. Kaul, “Hamiltonian models of lattice fermions solvable by the meron-cluster algorithm,” *Phys. Rev. D* **103**, 054033 (2021), [arXiv:2011.13208](https://arxiv.org/abs/2011.13208) [hep-lat].

[17] Debasish Banerjee, “Recent progress on cluster and meron algorithms for strongly correlated systems,” *Indian J. Phys.* **95**, 1669–1680 (2021), [arXiv:2101.03161](https://arxiv.org/abs/2101.03161) [hep-lat].

[18] S. Chandrasekharan, J. Cox, J.C. Osborn, and U.-J. Wiese, “Meron-cluster approach to systems of strongly correlated electrons,” *Nuclear Physics B* **673**, 405–436 (2003).

[19] Debasish Banerjee and Emilie Huffman, “Quantum Monte Carlo for gauge fields and matter without the fermion determinant,” *Phys. Rev. D* **109**, L031506 (2024), [arXiv:2305.08917](https://arxiv.org/abs/2305.08917) [hep-lat].

[20] Joao C. Pinto Barros, Thea Budde, and Marina Krstic Marinkovic, “Meron-Cluster Algorithms for Quantum Link Models,” *PoS LATTICE2023*, 024 (2024), [arXiv:2402.01039](https://arxiv.org/abs/2402.01039) [hep-lat].

[21] E. A. Martinez *et al.*, “Real-time dynamics of lattice gauge theories with a few-qubit quantum computer,” *Nature* **534**, 516–519 (2016), [arXiv:1605.04570](https://arxiv.org/abs/1605.04570) [quant-ph].

[22] Hannes Bernien, Sylvain Schwartz, Alexander Keesling, Harry Levine, Ahmed Omran, Hannes Pichler, Soon-won Choi, Alexander S. Zibrov, Manuel Endres, Markus Greiner, and et al., “Probing many-body dynamics on a 51-atom quantum simulator,” *Nature* **551**, 579–584 (2017).

[23] Sepehr Ebadi *et al.*, “Quantum phases of matter on a 256-atom programmable quantum simulator,” *Nature* **595**, 227–232 (2021), [arXiv:2012.12281](https://arxiv.org/abs/2012.12281) [quant-ph].

[24] Bing Yang, Hui Sun, Robert Ott, Han-Yi Wang, Torsten V. Zache, Jad C. Halimeh, Zhen-Sheng Yuan, Philipp Hauke, and Jian-Wei Pan, “Observation of gauge invariance in a 71-site Bose–Hubbard quantum simulator,” *Nature* **587**, 392–396 (2020), [arXiv:2003.08945](https://arxiv.org/abs/2003.08945) [cond-mat.quant-gas].

[25] Zhao-Yu Zhou, Guo-Xian Su, Jad C. Halimeh, Robert Ott, Hui Sun, Philipp Hauke, Bing Yang, Zhen-Sheng Yuan, Jürgen Berges, and Jian-Wei Pan, “Thermalization dynamics of a gauge theory on a quantum simulator,” *Science* **377**, abl6277 (2022), [arXiv:2107.13563](https://arxiv.org/abs/2107.13563) [cond-mat.quant-gas].

[26] Giulia Semeghini *et al.*, “Probing topological spin liquids on a programmable quantum simulator,” *Science* **374**, abi8794 (2021), [arXiv:2104.04119](https://arxiv.org/abs/2104.04119) [quant-ph].

[27] M. Schuyler Moss, Sepehr Ebadi, Tout T. Wang, Giulia Semeghini, Annabelle Bohrdt, Mikhail D. Lukin, and Roger G. Melko, “Enhancing variational Monte Carlo simulations using a programmable quantum simulator,” *Phys. Rev. A* **109**, 032410 (2024), [arXiv:2308.02647](https://arxiv.org/abs/2308.02647) [cond-mat.quant-gas].

[28] Daniel Gonzalez-Cuadra *et al.*, “Observation of string breaking on a (2 + 1)D Rydberg quantum simulator,” *Nature* **642**, 321–326 (2025), [arXiv:2410.16558](https://arxiv.org/abs/2410.16558) [quant-ph].

[29] Julian Schuhmacher, Guo-Xian Su, Jesse J. Osborne, Anthony Gandon, Jad C. Halimeh, and Ivano Tavernelli, “Observation of hadron scattering in a lattice gauge theory on a quantum computer,” (2025), [arXiv:2505.20387](https://arxiv.org/abs/2505.20387) [quant-ph].

[30] Jesús Cobos, Joana Fraxanet, César Benito, Francesco di Marcantonio, Pedro Rivero, Kornél Kapás, Miklós Antal Werner, Örs Legeza, Alejandro Bermudez, and Enrique Rico, “Real-Time Dynamics in a (2+1)-D Gauge Theory: The Stringy Nature on a Superconducting Quantum Simulator,” (2025), [arXiv:2507.08088](https://arxiv.org/abs/2507.08088) [quant-ph].

[31] De Luo *et al.*, “Quantum simulation of bubble nucleation across a quantum phase transition,” (2025), [arXiv:2505.09607](https://arxiv.org/abs/2505.09607) [quant-ph].

[32] Zohreh Davoudi, Chung-Chun Hsieh, and Saurabh V. Kadam, “Quantum computation of hadron scattering in a lattice gauge theory,” (2025), [arXiv:2505.20408](https://arxiv.org/abs/2505.20408) [quant-ph].

[33] Natalie Klco, Jesse R. Stryker, and Martin J. Savage, “SU(2) non-Abelian gauge field theory in one dimension on digital quantum computers,” *Phys. Rev. D* **101**, 074512 (2020), [arXiv:1908.06935](https://arxiv.org/abs/1908.06935) [quant-ph].

[34] Sandip Maiti, Debasish Banerjee, Bipasha Chakraborty, and Emilie Huffman, “Spontaneous symmetry breaking in a SO(3) non-Abelian lattice gauge theory in 2+1D with quantum algorithms,” *Phys. Rev. Res.* **7**, 013283 (2025), [arXiv:2409.07108](https://arxiv.org/abs/2409.07108) [hep-lat].

[35] Federica M. Surace, Paolo P. Mazza, Giuliano Giudici, Alessio Lerose, Andrea Gambassi, and Marcello Dalmonte, “Lattice gauge theories and string dynamics in rydberg atom quantum simulators,” *Phys. Rev. X* **10**, 021041 (2020).

[36] S Chandrasekharan, “Quantum link models: A discrete approach to gauge theories,” *Nuclear Physics B* , 17 (1997).

[37] R. Brower, S. Chandrasekharan, and U. J. Wiese, “QCD as a quantum link model,” *Physical Review D: Particles and Fields* **60**, 094502 (1999), [arXiv:hep-th/9704106](https://arxiv.org/abs/hep-th/9704106).

[38] Uwe-Jens Wiese, “From quantum link models to d-theory: A resource efficient framework for the quantum simulation and computation of gauge theories,” (2021), [arXiv:2107.09335](https://arxiv.org/abs/2107.09335) [hep-lat].

[39] Michael Hermele, Matthew P. A. Fisher, and Leon Balents, “Pyrochlore photons: The U (1) spin liquid in a S=12 three-dimensional frustrated magnet,” *Phys. Rev. B* **69**, 064404 (2004), [arXiv:cond-mat/0305401](https://arxiv.org/abs/cond-mat/0305401).

[40] Roderich Moessner and Kumar S. Raman, “Quantum dimer models,” (Springer Berlin Heidelberg, 2010) pp. 437–479.

[41] D. Banerjee, F. J. Jiang, P. Widmer, and U. J. Wiese, “The (2 + 1)-d U(1) quantum link model masquerading as deconfined criticality,” *Journal of Statistical Mechanics: Theory and Experiment* **1312**, P12010 (2013), [arXiv:1303.6858](https://arxiv.org/abs/1303.6858) [cond-mat.str-el].

[42] D. Banerjee, M. Bögli, C. P. Hofmann, F.-J. Jiang, P. Widmer, and U.-J. Wiese, “Interfaces, strings, and a soft mode in the square lattice quantum dimer model,” *Physical Review B* **90**, 245143 (2014).

[43] A. Banerjee, D. Banerjee, G. Kanwar, A. Mariani, T. Rindlisbacher, and U. J. Wiese, “Broken symmetry and fractionalized flux strings in a staggered U(1) pure gauge theory,” *Phys. Rev. D* **109**, 014506 (2024), [arXiv:2309.17109 \[hep-lat\]](#).

[44] Torsten V. Zache, Maarten Van Damme, Jad C. Halimeh, Philipp Hauke, and Debasish Banerjee, “Toward the continuum limit of a (1+1)D quantum link schwinger model,” *Phys. Rev. D* **106**, L091502 (2022).

[45] Lorenzo Cardarelli, Sebastian Greschner, and Luis Santos, “Deconfining disordered phase in two-dimensional quantum link models,” *Phys. Rev. Lett.* **124**, 123601 (2020), [arXiv:1910.12829 \[cond-mat.quant-gas\]](#).

[46] Tomohiro Hashizume, Jad C. Halimeh, Philipp Hauke, and Debasish Banerjee, “Ground-state phase diagram of quantum link electrodynamics in (2+1)-d,” *SciPost Phys.* **13**, 017 (2022), [arXiv:2112.00756 \[cond-mat.str-el\]](#).

[47] N. S. Srivatsa, Jesse J. Osborne, Debasish Banerjee, and Jad C. Halimeh, “Bosonic vs. Fermionic Matter in Quantum Simulations of 2 + 1D Gauge Theories,” (2025), [arXiv:2504.17000 \[cond-mat.str-el\]](#).

[48] A. Bashir, A. Raya, I. C. Cloet, and C. D. Roberts, “Regarding confinement and dynamical chiral symmetry breaking in QED3,” *Phys. Rev. C* **78**, 055201 (2008), [arXiv:0806.3305 \[hep-ph\]](#).

[49] F. F. Assaad and Tarun Grover, “Simple Fermionic Model of Deconfined Phases and Phase Transitions,” *Phys. Rev. X* **6**, 041049 (2016), [arXiv:1607.03912 \[cond-mat.str-el\]](#).

[50] Shai M. Chester and Silviu S. Pufu, “Anomalous dimensions of scalar operators in QED<sub>3</sub>,” *JHEP* **08**, 069 (2016), [arXiv:1603.05582 \[hep-th\]](#).

[51] Silviu S. Pufu and Subir Sachdev, “Monopoles in 2 + 1-dimensional conformal field theories with global U(1) symmetry,” *JHEP* **09**, 127 (2013), [arXiv:1303.3006 \[hep-th\]](#).

[52] Rufus Boyack, Ahmed Rayyan, and Joseph Maciejko, “Deconfined criticality in the QED3 Gross-Neveu-Yukawa model: The 1/N expansion revisited,” *Phys. Rev. B* **99**, 195135 (2019), [arXiv:1812.02720 \[cond-mat.str-el\]](#).

[53] Xiao Yan Xu, Yang Qi, Long Zhang, Fakher F. Assaad, Cenke Xu, and Zi Yang Meng, “Monte carlo study of lattice compact quantum electrodynamics with fermionic matter: The parent state of quantum phases,” *Phys. Rev. X* **9**, 021022 (2019).

[54] Jesse J. Osborne, Ian P. McCulloch, Bing Yang, Philipp Hauke, and Jad C. Halimeh, “Large-scale 2 + 1D U(1) gauge theory with dynamical matter in a cold-atom quantum simulator,” *Communications Physics* **8**, 273 (2025), [arXiv:2211.01380 \[cond-mat.quant-gas\]](#).

[55] Sriram Bharadwaj, Emil Rosanowski, Simran Singh, Alice di Tucci, Changnan Peng, Karl Jansen, Lena Funcke, and Di Luo, “A Path to Quantum Simulations of Topological Phases: (2+1)D Wilson Fermions Coupled To U(1) Background Gauge Fields,” *arXiv e-prints*, [arXiv:2504.21828 \(2025\)](#), [arXiv:2504.21828 \[hep-lat\]](#).

[56] Arianna Crippa, Karl Jansen, and Enrico Rinaldi, “Analysis of the confinement string in (2 + 1)-dimensional Quantum Electrodynamics with a trapped-ion quantum computer,” *arXiv e-prints*, [arXiv:2411.05628 \(2024\)](#), [arXiv:2411.05628 \[hep-lat\]](#).

[57] Michael Creutz, “Emergent spin,” *Annals Phys.* **342**, 21–30 (2014), [arXiv:1308.3672 \[hep-lat\]](#).

[58] S. Chandrasekharan, J. Cox, K. Holland, and U.-J. Wiese, “Meron-cluster simulation of a chiral phase transition with staggered fermions,” *Nuclear Physics B* **576**, 481–500 (2000).

[59] Cornelius Lanczos, “An iteration method for the solution of the eigenvalue problem of linear differential and integral operators,” *Journal of research of the National Bureau of Standards* **45**, 255–282 (1950).

## Supplementary Material

### Global and Gauge Symmetries

We discuss the global symmetries of the Hamiltonian (see also eq. (1)):

$$H = -t \sum_{x,i} \left[ \left( \psi_x^\dagger U_{x,i} \psi_{x+\hat{i}} + \text{h.c.} \right) - E_{x,\hat{i}} (n_{x+\hat{i}} - n_x) \right] + (V-t) \sum_{x,i} \left( n_x - \frac{1}{2} \right) \left( n_{x+\hat{i}} - \frac{1}{2} \right) - \frac{t \cdot d \cdot \mathcal{V}}{4}. \quad (3)$$

which is split into different superselection sectors labelled via local charges labelled by the Gauss Law (see also eq. (2)):

$$G_x = n_x + \left( \frac{(-1)^x - 1}{2} \right) - \sum_i (E_{x,\hat{i}} - E_{x-\hat{i},\hat{i}}), \quad (4)$$

Note that this differs from the usual staggered fermion formulation by omitting the staggered phase  $\eta_{x,i} = (-1)^{\sum_{j < i} x_j}$  in the kinetic energy term for the hopping fermions; where we have used the notation  $x = (x_1, x_2, \dots, x_d)$ . While the  $\eta$  phase is included to ensure relativistic dispersion for fermions in pure fermionic theories, this seems to be not essential when gauge fields are coupled to the fermions [53, 57].

The major discrete symmetry that plays a key role in our analysis is the shift symmetry,  $\mathcal{S}_k$ , which is a discrete translation of all fields by one lattice unit along the  $k$ -th spatial direction. This is the discrete chiral symmetry for this model. The symmetry is implemented on the operators as:

$$\mathcal{S}^k \psi_x = \psi_{x+\hat{k}}, \mathcal{S}^k U_{x,\hat{i}} = U_{x+\hat{k},\hat{i}}, \mathcal{S}^k E_{x,\hat{i}} = E_{x+\hat{k},\hat{i}}. \quad (5)$$

However, under the action of eq. (5), the Gauss law operator at site  $x$  transforms as,

$$G_x \xrightarrow{\mathcal{S}^k} G_{x+\hat{k}} + (-1)^x. \quad (6)$$

This necessitates the need of the two-site labelling used in the paper. Under this transformation, each Fock state in the Gauss law sector  $G(e, o) = (0, 0), (2, -2), (3, -3)$  is mapped to a unique Fock states in a corresponding GL sector,  $(1, -1), (-1, 1), (-2, 2)$  respectively. These sectors related by the shift symmetry  $\mathcal{S}^k$  and are therefore physically equivalent since the two sectors are isomorphic. Further, in  $d > 1$ , shifts by single lattice spacings in two *different* directions generate a discrete  $\mathbb{Z}_2$  flavour symmetry.

Shifts by two lattice spacings in the same direction generate the usual *translation* symmetry,  $T_k$ , in the  $k$ -th direction. In addition, we have usual discrete rotational symmetries, either by a  $\pi$ -rotation or a  $\pi/2$  rotation depending on whether the system is rectangular or a square.

Finally, charge conjugation is an internal symmetry: for staggered fermions, this is defined acting in a particular direction, as follows:

$$\mathcal{C}^k \psi_x = \psi_{x+\hat{k}}^\dagger, \mathcal{C}^k U_{x,\hat{i}} = U_{x+\hat{k},\hat{i}}^\dagger, \mathcal{C}^k E_{x,\hat{i}} = -E_{x+\hat{k},\hat{i}}. \quad (7)$$

The different phases realized in the regimes studied break either the shift symmetry for large values of  $V/t$  or the point group symmetry (the translation and rotational symmetries) at large negative values of  $V/t$ , as discussed in the main text. Finite size scaling of energy gaps as a diagnostic for these phases are discussed in the last section of this appendix.

### Solutions in different GL sectors

For the square lattice, the local constraint  $n - \nabla \cdot E = g$  restricts the allowed electric field values on the  $2d$  links around a site, with the admissible configurations determined by  $n - g$  and by whether the site is even or odd. For the GL sector  $(2, -2)$ , the local Hilbert space is constructed by solving  $n - \nabla \cdot E = 2$  on even sites and  $n - 1 - \nabla \cdot E = -2$  on odd sites. The first equation gives 1 (4) allowed solutions with  $n = 0$  ( $n = 1$ ) on even sites, while the second equation yields 4 (1) solutions for  $n = 0$  ( $n = 1$ ) on odd sites, resulting in (5, 5) allowed solutions on (even, odd) sites for  $d = 2$ . In the shifted GL sector  $(-1, 1)$ , the Gauss law equations on even and odd sites are swapped relative to the sector  $(2, -2)$ , that leads to the same number of solutions.

In case of the cubic lattice  $d = 3$ , each site is connected with six links, producing an unconstrained Hilbert space of dimension  $2^6$  before the Gauss law constraints are imposed. The GL sectors related by shift symmetry are  $[(0, 0) \text{ and } (1, -1)], [(2, -2) \text{ and } (-1, 1)], [(3, -3) \text{ and } (-2, 2)]$ . For the GL sector  $(0, 0)$ , putting  $G = 0$  into the above Gauss law constraint equations fixes the required divergence on even (odd) sites. Counting all six link electric field configurations consistent with these conditions gives 20 (15) states for  $n = 0$  ( $n = 1$ ) on even sites and 15 (20) on odd sites, yielding in total 35 (35) solution for even (odd) sites for this sector. Similarly, the sector  $(1, -1)$  also has 35 (35) solutions for even (odd) sites. For the sector  $(2, -2)$  we obtain 21 (21) and for the sector  $(3, -3)$  we get 7 (7) solutions. There is another GL sector  $(4, -4)$  (and its shifted partner  $(-3, 3)$ ) where there is a single state of completely frozen fermions which do not hop at all.

How do we know that we have considered all the GL sectors? This can be argued through a general counting formula. Consider a hypercubic lattice in spatial dimension  $d$ , so each site touches  $2d$  links. The total number of all possible local states is

$$N_{\text{total}}(d) = 2^{2d} = \sum_{k=-d}^d \binom{2d}{d+k}, \quad (8)$$

spread across all possible GL sectors. Each link  $S_\ell^z = \pm 1/2$ . With our GL conventions, for a fixed value of the local GL  $g$  and a fixed matter occupation  $n_x$ , the number of local solutions are

$$N(d, g, n_x) = \binom{2d}{d + n_x - g} \quad (9)$$

where  $\nabla \cdot E = n_x - g$ . The total number of solutions in a sector can be obtained by summing over  $n_x = 0, 1$ . For example, in  $d = 3$ , this gives it gives 35, 21, 7, 1 solutions for GL sector  $(0, 0)$ ,  $(2, -2)$ ,  $(3, -3)$ , and  $(4, -4)$  respectively, consistent with the local Gauss law constraints. This clearly also implies that these are all the possible solutions since they add up to  $64 = 2^6$ , which are all the possible link orientations for the electric fluxes in this representation.

### Sign problem in different GL sectors

In the main text, we discussed a procedure on how to examine whether a particular GL sector suffers from a sign problem. Using this procedure, we now demonstrate that the physical sector of interest to particle physics, which is often taken to be  $(0, 0)$ , suffers from a sign problem in both  $d = 2, 3$ . The proof is outlined pictorially in fig. 7, which attempts to switch the position of two fermions in a configuration keeping the location of all other fermions fixed.

### Cluster Algorithm

In this subsection, we discuss the construction of the quantum Monte Carlo algorithm, which was used to obtain results for larger lattices. The algorithm is constructed in terms of worldline configurations of the fermion occupation basis ( $n_x$ ) and the electric-flux ( $s^3 = E$ ) basis for the gauge links. In any dimension, the Hamiltonian is decomposed into a set of operators, such that operators in each set mutually commute. In  $d = 3$ , the Hamiltonian is decomposed into six components,

$$H = H_1 + H_2 + H_3 + H_4 + H_5 + H_6, \quad (10)$$

with

$$H_i = \sum_{\substack{x=(x_1, x_2, x_3) \\ x_i \in \text{even}}} h_{x,i}, \quad H_{i+3} = \sum_{\substack{x=(x_1, x_2, x_3) \\ x_i \in \text{odd}}} h_{x,i}. \quad (11)$$

This Suzuki-Trotter decomposition [58] allows an expansion of the Boltzmann operator  $\exp(-\beta H)$  across  $2dN_t = \beta$  discrete Euclidean time slices of spacing  $\epsilon = \frac{\beta}{N_t}$ . The

partition function then takes the form

$$\begin{aligned} Z &= \text{Tr}(e^{-\beta H}) \\ &= \sum_{\{s,n\}} \prod_{\tau} \langle s(x, \tau), n(x, \tau) | e^{-\epsilon H_1} \\ &\quad \cdots e^{-\epsilon H_6} | s(x, \tau - 1), n(x, \tau - 1) \rangle, \end{aligned} \quad (12)$$

where  $|s(x, 0), n(x, 0)\rangle = |s(x, \beta), n(x, \beta)\rangle$ . In this representation, the occupied sites define the fermion worldline that are closed in Euclidean time, and electric flux variables track the gauge field dynamics. Each Trotter slice encodes a local configuration of fermion occupation and link variable, and the sequential operation of the transfer matrix,  $e^{-\epsilon H_i}$ , generates the full worldline ensemble. These worldline configurations form the basis for constructing clusters. Evaluating the matrix elements of the transfer matrix allows the partition function to be expressed in terms of a local action and sign factor, where the contribution from each plaquette takes the form

$$W_{\text{plaq}} = e^{-S[n(x, \tau), n(x+i, \tau), n(x, \tau+1), n(x+i, \tau+1); s^3(x, \tau), s^3(x, \tau+1)]}, \quad (13)$$

$$Z = \prod_{x, \tau} \sum_{n(x, \tau), s^3(x, \tau)} \text{sign} [\{n\}] W_{\text{plaq}}. \quad (14)$$

Here, the local action  $S[n(x, \tau), n(x+i, \tau), n(x, \tau+1), n(x+i, \tau+1); s^3(x, \tau), s^3(x, \tau+1)]$  couples the fermion occupations on neighbour sites at  $\tau$  with their neighbours in  $\tau + 1$ , as well as the corresponding electric flux variables in these time slices, while  $\text{sign} [\{n\}]$  tracks negative signs while for fermionic worldlines. Each active plaquette (shaded in gray) must correspond to one of the configurations listed in fig. 8. The weight of plaquette is computed from the local matrix elements  $\langle s_b, n_b | e^{-\epsilon H_b} | s'_b, n'_b \rangle$ , where  $b$  is a nearest-neighbor bond,  $b = \{x, x+i\}$ . By introducing appropriate breakups associated with each plaquette, the matrix element products from eq. (12) can be decomposed into clusters, which preserve the allowed local configurations while maintaining detailed balance.

*Breakup* is a technical term indicating that a subset of the six degrees of freedom in an active plaquette (four fermions at the two corners, and two gauge fluxes in the joining bonds) are connected together in a manner that satisfies detailed balance and can be updated simultaneously. Breakups can be of different types, which connect different subsets. For example, in order to satisfy detailed balance, the A, D and E breakups shown in fig. 8, need to be applied with a probability given by eq. (15) for  $V \geq 2t$ . Once breakups are applied at all active plaquettes in a configuration, one can define a cluster as the set of all fermions and gauge links which are connected together. Meron clusters, or merons, are those which on flipping changes the sign of weight of the configurations.

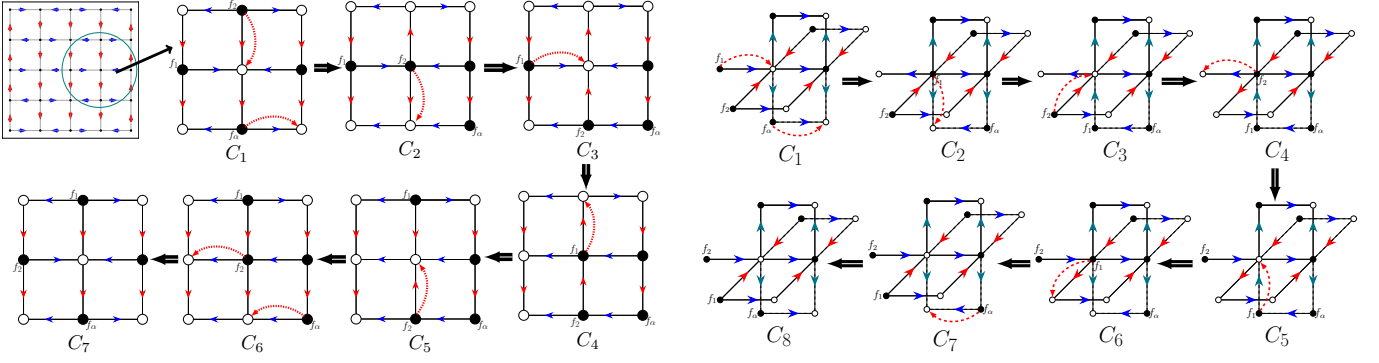


Figure 7. The GL constraints in the sector  $(0, 0)$  in  $d = 2$  (left) and  $d = 3$  (right) are relaxed enough to allow fermions  $f_1$  and  $f_2$  to exchange positions with each other following giving rise to the fermion sign problem in these sectors.

| Plaquettes | Weights               | Breakups |
|------------|-----------------------|----------|
|            | $\exp(-\epsilon V/2)$ |          |
|            | $\exp(-\epsilon t)$   |          |
|            | $\cosh(\epsilon t)$   |          |
|            | $\sinh(\epsilon t)$   |          |

Figure 8. Breakup and corresponding weights for the spin- $\frac{1}{2}$   $U(1)$  gauge links coupled with matter Hamiltonian in eq. (1).

In this formulation, the link variables also contribute, either as additional lines in the A breakup or as binding extensions in the D and E breakups, representing a key generalization of the original meron cluster algorithm to gauge theories.

$$\begin{aligned} W_A &= \exp(-\epsilon V/2) \\ W_D &= \sinh(\epsilon t) \\ W_E &= \exp(-\epsilon t) - \exp(-\epsilon V/2). \end{aligned} \quad (15)$$

Flipping a cluster is defined as an operation that exchanges the occupied (up) and empty (down) sites (links). If a cluster is flipped, the magnitude of the weights of configuration remain the same. But if the cluster flip changes the sign of the configuration, it is a meron. Rules for identifying a cluster as a meron are given in the next section. With a certain choice of breakups it is possible to factorize the sign factor of a configuration  $C$  into a product of the signs of each cluster,  $\text{Sign}[C] = \prod_{i=1}^{N_c} \text{Sign}[C_i]$ , where  $C$  decomposes into  $N_c$  clusters. By suitably flipping the clusters, one can

reach the reference configuration with  $\text{Sign} = 1$ . The QMC update is as follows:

1. Start from the reference configuration that contains only the fermion worldlines. Choose an active plaquette randomly.
2. If a random plaquette can switch to a different breakup, change it with a probability based on its breakup weight.
3. After a breakup is modified, re-examine the resulting configuration. If the modification leads to merons in the configuration, then restore the breakup to its previous state and return to step 2.
4. For each cluster, flip all fermion occupations and flux variables with probability  $1/2$ .

### Meron rule

For spinless non-relativistic fermions, the rule [15] of identifying a meron cluster is,

$$\begin{aligned} n_w + \frac{n_h}{2} &= \text{even}, & \text{PBC} \\ n_w + \frac{n_h}{2} &= \text{odd}, & \text{APBC.} \end{aligned} \quad (16)$$

where,  $n_w$  is the temporal winding number of the cluster,  $n_h$  is the number of hops that the cluster makes to neighboring sites while the cluster encounters horizontal bonds (D-breakup or E-breakup). PBC and APBC are periodic and anti-periodic boundary conditions, respectively. When coupled to  $U(1)$  gauge fields, the presence of gauge fields allows multiple fermion loops to become bound together through the gauge link variables. In that case, the following meron definition rules [19] work for

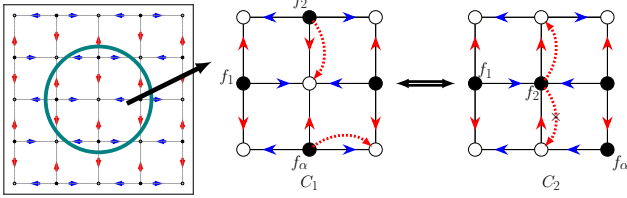


Figure 9. In the Ground-state configuration of the Gauss law sector  $G(2, -2)$  in 2-d, the orientation of gauge links restricts the hopping of the fermions  $f_1$  and  $f_2$  to at most one lattice spacing, which implies that position of fermions cannot be exchanged by the action of Hamiltonian.

PBC,

$$\begin{aligned} n_w + \frac{n_h}{2} &= \text{even,} & \text{odd \# of loops} \\ n_w + \frac{n_h}{2} &= \text{odd,} & \text{even \# of loops.} \end{aligned} \quad (17)$$

If a cluster contains one fermion loop, the number of loops is odd and the first equation of eq. (17) applies. The condition then reduces to eq. (16), reproducing the meron rule for the purely fermionic case. In  $d = 2, 3$ , the ground state has no merons, as illustrated in main text and also in fig. 9. This indicates that the  $G(2, -2)$  sector in 2-d is free from the fermionic sign problem.

#### Check with ED

We have implemented the meron cluster algorithm in both  $d = 2$  and  $d = 3$  and benchmarked the quantum Monte-Carlo code with the exact diagonalization (ED) result in both cases. Naturally, the ED works for small lattice sizes, since the number of Fock states increase exponentially. For lattice sizes  $2 \times 8$ ,  $4 \times 4$ , and  $2 \times 2 \times 2$ , it is easy to do the full ED. For larger systems, we used a Krylov-based framework. We constructed the Fock states within the Krylov subspace and performed diagonalization using the Lanczos algorithm [59] for the lowest 100 states, and then monitored the convergence of the eigenvalues as a function of the number of Krylov subspaces. The results displayed in our plots for larger lattices only show results which have fully converged. The convergence is at least  $10^{-4}$  for lattices smaller than the  $2 \times 10$  lattice, while an accuracy of  $10^{-3}$  is reached for the larger lattices  $2 \times 12$ ,  $4 \times 6$ . Of course, for smaller lattice where full ED could be used, we have machine-precision results.

| $L_x \times L_y$ | $(0,0)$ |             | $(2, -2)$ |             |
|------------------|---------|-------------|-----------|-------------|
|                  | k-iter  | # of states | k-iter    | # of states |
| $2 \times 10$    | 4       | 17456       | 10        | 891097      |
|                  | 6       | 238467      |           |             |
|                  | 7       | 686977      |           |             |
|                  | 8       | 1744187     |           |             |
|                  | 9       | 3984067     |           |             |
|                  | 10      | 8298344     |           |             |
|                  | 11      | 15935644    |           |             |
|                  | 12      | 28439159    |           |             |
|                  | 13      | 47474769    |           |             |
|                  | 14      | 74495344    |           |             |
|                  | 3       | 5935        |           |             |
|                  | 4       | 39670       |           |             |
|                  | 5       | 199198      |           |             |
| $2 \times 12$    | 6       | 807368      | 12        | 13800964    |
|                  | 7       | 2773220     |           |             |
|                  | 8       | 8320787     |           |             |
|                  | 9       | 22280495    |           |             |
|                  | 4       | 35254       |           |             |
| $4 \times 6$     | 5       | 165754      | 12        | 8205424     |
|                  | 6       | 630644      |           |             |
|                  | 7       | 2048564     |           |             |
|                  | 8       | 5853611     |           |             |
|                  | 9       | 15026683    |           |             |
|                  | 10      | 35186815    |           |             |
|                  | 11      | 75957235    |           |             |
|                  | 12      | 152451955   |           |             |
|                  | 13      | 286253539   |           |             |
|                  | 3       | 21016       | 3         | 47869       |
| $6 \times 6$     | 4       | 220825      | 4         | 637027      |
|                  | 5       | 1723735     | 5         | 6023779     |
|                  | 6       | 10572547    | 6         | 41850295    |
|                  | 7       | 53331511    | 7         | 218048551   |
|                  | 8       | 863252872   |           |             |

Table I. The number of allowed states in the  $G(e, o)$  sectors in 2D under krylov space expansion.

Let us give an estimate of the matrix sizes involved in the procedure. The unconstrained Hamiltonian with

spin- $\frac{1}{2}$  gauge links coupled to matter on a lattice of volume  $\mathcal{V} = L_x \times L_y$  in 2D and  $\mathcal{V} = L_x \times L_y \times L_z$  in 3D contains  $2^{3 \times \mathcal{V}}$  and  $2^{4 \times \mathcal{V}}$  possible configurations respectively. Imposing the Gauss law constraints in order to select sectors defined by  $(G_e, G_o)$ , significantly reduces the Hilbert space dimension. In our simulations, we focus on the Gauss law sectors  $(0, 0)$  and  $(2, -2)$  in  $d = 2$ , and  $(0, 0)$ ,  $(2, -2)$ , and  $(3, -3)$  in  $d = 3$ . The corresponding accessible Hilbert space dimensions obtained via this method are listed in table I and table II.

| $L_x \times L_y \times L_z$ | $(0,0)$ | $(2, -2)$<br>k-iter | # of states |
|-----------------------------|---------|---------------------|-------------|
| $2 \times 2 \times 2$       | 303721  |                     | 42393       |
|                             |         | 10                  | 22009434    |
| $2 \times 2 \times 4$       |         | 12                  | 85532652    |
|                             |         | 15                  | 377993792   |

Table II. The number of allowed states in the  $G(e, o)$  sectors in 3D.

We have checked the following observables against ED calculations with results computed using the Monte Carlo algorithm. The results are summarized in table III, table IV for  $V = 2t$  in  $d = 2$  and  $d = 3$  respectively, and in fig. 10 with  $V/t$  in  $d = 2$ . All observables are evaluated in the ground state Gauss law sector  $G(e, o) = (2, -2)$  in  $d = 2$  and  $G(e, o) = (3, -3)$  in  $d = 3$  respectively.

$$\begin{aligned}
 \psi^\dagger \psi &= \frac{1}{L_t} \sum_{x,t} (-1)^x n_x \\
 \epsilon_\mu &= \frac{1}{L_t} \sum_{x,t} (-1)^x S_{x,x+\hat{\mu}}^3, \quad \mu, \nu = 1, 2, \dots, D \\
 \mathcal{O} &= \frac{1}{L_t} \sum_{x,t} (U_\square + U_\square^\dagger), \quad U_\square = U_{x,\mu} U_{x+\hat{\mu},\nu} U_{x+\hat{\nu},\mu}^\dagger U_{x,\nu}^\dagger
 \end{aligned} \tag{18}$$

| $L_x \times L_y$ |    | $\langle \psi^\dagger \psi \rangle$ | $\langle \epsilon_x \rangle$ | $\langle \epsilon_y \rangle$ | $\langle \mathcal{O} \rangle$ |
|------------------|----|-------------------------------------|------------------------------|------------------------------|-------------------------------|
| $2 \times 6$     | ED | -4.8682                             | -5.6576                      | -5.7765                      | 0.02395                       |
|                  | MC | -4.8681(5)                          | -5.6575(3)                   | -5.7766(1)                   | 0.02396(5)                    |
| $2 \times 8$     | ED | -6.4909                             | -7.5435                      | -7.7020                      | 0.03193                       |
|                  | MC | -6.4912(6)                          | -7.5433(3)                   | -7.7023(2)                   | 0.03199(9)                    |
| $4 \times 4$     | ED | -6.72205                            | -7.6805                      | -7.6805                      | 0.01816                       |
|                  | MC | -6.7221(12)                         | -7.6804(4)                   | -7.6807(5)                   | 0.01812(8)                    |
| $2 \times 12$    | ED | -9.736                              | -11.315                      | -11.553                      | 0.0479                        |
|                  | MC | -9.737(2)                           | -11.316(1)                   | -11.552(1)                   | 0.0480(1)                     |
| $4 \times 6$     | ED | -10.085                             | -11.5206                     | -11.5217                     | 0.02716                       |
|                  | MC | -10.084(1)                          | -11.5203(3)                  | -11.5219(2)                  | 0.02723(5)                    |

Table III. Comparison of Meron Cluster(MC) values with the ED values for the observables  $\langle \psi^\dagger \psi \rangle$ ,  $\langle \epsilon_x \rangle$ ,  $\langle \epsilon_y \rangle$  and  $\langle \mathcal{O} \rangle$  for  $d = 2$ , and defined in eq. (18).

| $L_x \times L_y \times L_z$ |    | $\langle \psi^\dagger \psi \rangle$ | $\langle \epsilon_x \rangle$ | $\langle \epsilon_y \rangle$ |
|-----------------------------|----|-------------------------------------|------------------------------|------------------------------|
| $2 \times 2 \times 2$       | ED | -3.529                              | -3.922                       | -3.922                       |
|                             | MC | -3.538(6)                           | -3.924(2)                    | -3.923(2)                    |
| $2 \times 2 \times 4$       | ED | -7.109                              | -7.841                       | -7.841                       |
|                             | MC | -7.125(11)                          | -7.841(5)                    | -7.843(3)                    |

Table IV. Comparison between meron-cluster (MC) and exact diagonalization (ED) results for the observables  $\langle \psi^\dagger \psi \rangle$ ,  $\langle \epsilon_x \rangle$  and  $\langle \epsilon_y \rangle$  for  $d = 3$  and defined in eq. (18).

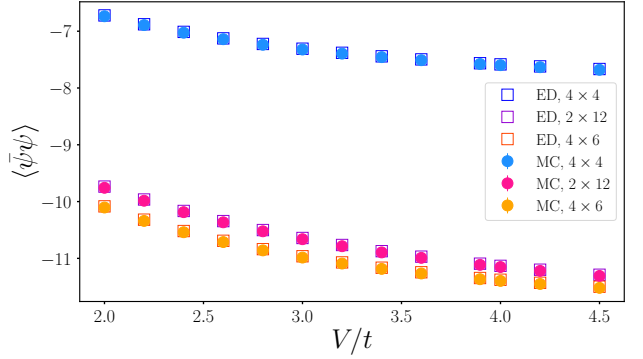


Figure 10. Comparison between meron-cluster (MC) and exact diagonalization (ED) results for the observable chiral condensate  $\langle \psi^\dagger \psi \rangle$  with interacting potential  $V/t$ .

### Finite size scaling in the phase diagram

In the main text, we provided a schematic outline of the phase diagram of the gauge theory with fermionic matter in both the GL sectors  $(2, -2)$  and  $(0, 0)$  in  $d = 2$ . We explain the physics of the different phases in some more detail in this subsection, by looking at the scaling of the mass gap in different regimes.

Let us consider the GL sector  $(2, -2)$  first. Based on our result from examining the nature of the sign problem, we know that since the fermions cannot hop more than one lattice spacing at a time, we expect the excitations to be gapped. Fig 11 shows the behaviour of the finite volume mass gap with volume in three different regimes  $V/t = -3.9, 0.0, 2.0$ . For  $V/t = -3.9$ , the mass gap vanishes, since this corresponds to a regime where the discrete rotation symmetry breaks spontaneously. Large negative values of  $V/t$  imply that Fock states where nearest neighbour states are both occupied or both empty form the ground state. However, all such states have domain walls separating regions which are completely filled with regions that are empty in order to maintain the half-filling. This simple considerations imply the existence of several degenerate ground state energies, and thus the gap vanishes, as seen in the panel showing the gap in

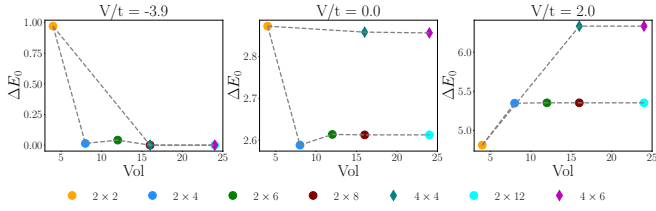


Figure 11. Finite volume scaling behaviour of the gap to the first excited state for fermionic matter in  $G(2, -2)$  sector for three different values of  $V/t$  corresponding to the three different phases described in the main text.

$V/t = -3.9$ .

Next, we consider the phase that is stabilized for  $V/t \sim 0$ . This is the region where the fermions can maximally hop, but never far. Consequently, the gap is finite and  $O(1)$ , and shows little finite volume effect. Interestingly, ladder systems with  $L_y = 2$  saturate to a slightly lower gap as compared to those with  $L_y = 4$ . It is likely that the phase is a massive  $Z_2$  gauge theory. For larger positive  $V/t$ , there is a unique charge density wave with staggered occupation which forms the ground state in the sector  $(2, -2)$ , and the orientation of the electric fluxes is set through the Gauss Law. The gap then corresponds to creating a single *dipole* defect by switching the occupation of an even-odd pair of sites and flipping the link between them, which is the action of the kinetic term. For a square lattice, this creates six *bad* bonds at which the energy due to the density-density interaction increases from  $-\frac{1}{4}$  to  $\frac{1}{4}$ , so  $6 \times \frac{1}{2} = 3$ . For the same six bonds, the designer term does not contribute any more compared to the ground state, while there is no additional change from the bond which was just flipped (since both the occupations and the electric flux orientation changes). This implies that we expect an excitation above the ground state with  $\Delta E \approx 6V/t$  in the strong coupling limit of  $V/t \rightarrow \infty$ . The observed value of slightly more than 6 is in the expected ballpark (note that the density-density term comes with a  $V - t$  coefficient). This calculation in the strong coupling limit suggests that such dipole defects are energetically unfavourable in this limit. Moreover, note that this calculation also suggests the phase to have massive quasi particles.

In a future publication, we will study the nature of the phase transition between these two phases using the

cluster algorithm. Another line of investigation is the case when the designer term is considered with opposite sign, which we also leave for the future. For the opposite sign of the designer term, creation of such dipole defects could be made favourable, thus triggering an instability of the ground state leading to a phase transition.

In the next figure, fig. 12, we show the corresponding finite size scaling of the mass gap for the same values  $V/t$  as in fig. 11. As in the case before, for negative values of  $V/t$  one will encounter domain wall states leading to several degenerate ground states and a vanishing of the mass gap. The significantly interesting case is the middle panel, for  $V/t = 0$ : the small mass gap for  $L_y = 2$  ladders decreases further for the  $4 \times 4$  lattice, indicating that a possibility exists for the system to have a light quasi particle mode in this region. This is consistent with the observation in [46], but studies on larger lattices are necessary to reach a conclusion. It is essential to develop the meron cluster algorithm to simulate this sector of the theory which has a genuine sign problem. For larger positive values of  $V/t$ , the scaling of the energy gap is similar, and we are unable to definitely conclude whether the system goes into a new phase based on this data alone. However, fig. 5 seem to indicate that diagonal observables (such as the chiral condensate and the staggered flux) saturate. This in turn indicates the existence of a different phase for  $V/t \gg 0$ . Since the mass gap is even lower in this regime, it could be the spontaneous breaking of a discrete symmetry. Note that the notion of *dipole excitations* in the  $(0, 0)$  GL sector is complicated by the fact that these sectors have flippable plaquettes. The presence of such flippable plaquettes can easily give rise to a closed flux excitation which makes a naive counting of bonds difficult.

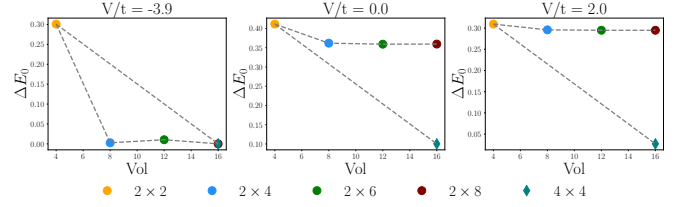


Figure 12. Finite volume scaling behaviour of the gap to the first excited state for the Fermionic case in  $G(0,0)$  sector for the same three values of  $V/t$  as in the last figure. These again correspond to different phases.